Neurocomputing 456 (2021) 609–621

Contents lists available at ScienceDirect

Neurocomputing

journal homepage: www.elsevier.com/locate/neucom

An intelligent system for harmonic distortions detection in wind generator power electronic devices

Esteban Jove [a], Jose Manuel González-Cava [b], José-Luis Casteleiro-Roca [a], Héctor Alaiz-Moretón [c], Bruno Baruque [d], Paulo Leitão [e], Juan Albino Méndez Pérez [b], José Luis Calvo-Rolle [a]

[a] University of A Coruña, CTC, Department of Industrial Engineering, CITIC Avda, 19 de febrero s/n, Ferrol, A Coruña 15405, Spain
[b] Universidad de La Laguna, Department of Computer Science and System Engineering, Avda. Astrofísico Francisco Sánchez, s/n, La Laguna 38200, Spain
[c] Universidad de León, Departamento de Ingeniería Eléctrica y de Sistemas y Automática, Edificio Tecnológico - Campus de Vegazana s/n, León 24071, Spain
[d] Universidad de Burgos, Departamento de Ingeniería Civil, Calle Francisco de Vitoria, s/n, Burgos 09006, Spain
[e] CeDRI - Research Centre in Digitalization and Intelligent Robotics, Polytechnic Institute of Bragança and INESC TEC, Porta, Portugal

ARTICLE INFO

Article history:
Received 20 March 2020
Revised 1 July 2020
Accepted 13 July 2020
Available online 18 June 2021

Keywords:
Energy efficiency
Wind generator
One-class
Outlier detection

ABSTRACT

The high concern about climate change has boosted the promotion of renewable energy systems, being the wind power one of the key generation possibilities in this field. In this context, with the aim of ensuring the energy efficiency, the present work deals with the fault detection in the power electronic circuits of a wind generator system placed in a bioclimatic house. To do so, different outliers that emulate harmonic distortion appearance are tested. To implement a system capable of detecting this anomalous situations, six different one-class techniques are used, whose performance is thoroughly analyzed, offering interesting performance.

1. Introduction

In recent years, the global energy system has undergone continuous changes towards the decarbonization, the decentralization of the generation and the electrification of the economy. These changes also involve the promotion of an active participation of the consumers who must become aware of the importance of the sustainable use of the natural resources. All these measures aimed at a real global energy transition have led to the development of different global agreements such as the proposed in the UN Climate Change Conference or the actions included in Horizon 2020. In Spain, this energy transition has been motivated, not only by a variation in the annual average of ton of coal, increasing from 53 €/ton in 2016 to 76 €/ton in 2018, but also by the increase in the CO2 emission rights price, from 5 € in 2016 to over 20 € in 2018 [1]. Therefore, a greater integration of the renewable energies together with the promotion of a more sustainable mobility and energy efficiency are required goals nowadays [2].

Regarding the global use of renewable sources for electricity generation, 25.6% of the total electricity generated in 2018 came from renewable resources [3]. This evidences a considerable increase in the generation of renewable energy compared with recent years [4,5]. Among the different renewable technologies, hydroelectric power has been largely used, representing the 16% of the total electricity generation. Recently, wind power generation has emerged as a potential source to cover the demand. The installed power has increased from 17 GW in 2000 to 591 GW in 2018 [6,7]. Recent published works estimate that 22.6% of the total energy demand in the world will be supplied by wind energy in 2030 [8], which represents a significant development, taking into consideration that it only represented a 4.8% in 2018 [9].

Focusing on the Spanish wind generation, this positive trend is also considerable. From 23 GW of wind power installed in 2015 (18.2% of total generation), the forecasts for 2030 estimates this value up to 40 GW (33.6%), in the more optimistic scenarios [10]. This trend in the evolution of the wind energy implies that the main efforts must focus on the optimization of the current designs for wind generation. A proper design of the turbine lets maximize the performance of the device, increasing the power generation [11]. Thus, the power generation may range from kilowatts for small consumers, to megawatts for large populations depending on the turbine design. There are two main types of turbines:

E-mail addresses: esteban.jove@udc.es (E. Jove), jgonzalc@ull.edu.es (J.M. González-Cava), jose.luis.casteleiro@udc.es (J.-L. Casteleiro-Roca), hector.moreton@unileon.es (H. Alaiz-Moretón), bbaruque@ubu.es (B. Baruque), pleitao@ipb.pt (P. Leitão), jamendez@ull.edu.es (J.A. Méndez Pérez), jlcalvo@udc.es (J.L. Calvo-Rolle)

https://doi.org/10.1016/j.neucom.2020.07.155
0925-2312/

horizontal-axis wind turbines (HAWT) widely used in most current applications, and vertical-axis wind turbines (VAWT) capable of producing electricity with lower wind speeds. Although VAWTs should be placed close to the ground, minor outages in electricity generation have been observed. In general, VAWTs are not only characterized by superior performance, but also exhibit a very simple design that is cost effective from both manufacturing and maintenance perspectives [12].

Regardless of the turbine type, this technology transforms the movement of the rotor produced by the wind into electricity through a generator. Thus, the wind emerges as the key factor for the energy production. A proportional relationship between the power generated by the generator and the cube of the wind speed has been reported [13]. However, wind is a variable resource that depends not only on the solar energy, but also on other factors such as the variations in the surface or the season. In addition, the wind speed varies continuously. This phenomenon, known as turbulence, must be taken into account for planning the energy production and the avoidance of possible damages in the plant [8].

The first wind energy facilities were based on the constant rotatory movement of the turbine to generate a fixed frequency sinewave by means of a gearbox. Then, a powerful breaking system was needed in case of heavy wind gusts, with the consequent increment in heat dissipation and mechanical deterioration. Then, this kind of facilities were replaced by new technologies that do not need a fixed frequency blades rotation. Two different are considered for this issue: the doubly fed induction generators (DFIG) [14] and the permanent magnet synchronous generators (PMSG) [15]. Both approaches make use of an AC to DC stage, followed to a DC to AC stage, ensuring a fixed frequency, although in DFIG topology the generator is coupled to the network.

As the use of renewable energy installations must substitute the conventional polluting generation methods, they should offer an efficient and sustainable performance. In this sense, the development of tools that ensure the systems optimization play a significant role [16]. This optimization can not be achieved without a correct system operation, which means that an early fault situation must be detected.

Then, this work faces the problem of detecting malfunctions in a wind turbine located in a bioclimatic building. These kind of facilities are nowadays implemented using a rectification and an inversion stage. These processes commonly presents problems with electric harmonic distortion, that reduces the real power generated by the system [17].

From a real dataset corresponding to the normal operation of a wind turbine facility, different novelty detection classifiers are implemented through six one-class techniques. These techniques aim to describe, from a training set, the behavior of the correct system operation, known as target class [18]. Then, all test samples that do not belong to this class are labeled as anomalies or faults [19].

According to different works [19,20], the anomaly detection can be carried out through three different basic ideas. The first idea tries to determine the geometric boundaries of the target set and, the anomaly is detected when the data is outside these boundaries [19]. The second method analyzes the density distribution of the training set and determines the novelty when the test data density is below a given threshold [18]. Finally, the possibility of implementing reconstruction models can be used to determine the fault appearance, based on the reconstruction error of a test sample [21].

This paper is structured as follows. Next section describes the case of study, that consists of a wind turbine located on a bioclimatic house. Then, Section 3 details the one-class techniques applied to achieve the anomaly detection. Experiments and results are described in Section 4 and discussed in Section 5. Finally, Section 6 exposes the conclusions and future works.

2. Case study

The main objective of this work is the proposal of a novel method for fault diagnosis due to electric harmonic distortion in wind turbines. In particular, this algorithm has been applied to detect malfunctions in a wind turbine installed in a bioclimatic house. Further details of the case of study are presented in the following subsections.

2.1. Energetic system description

This study analyzes the wind generator installed in the bioclimatic house of Sotavento, in the Sotavento Experimental Wind Farm (Lugo, Spain). It was founded by the Sotavento Galicia Foundation to study the impact of using renewable energy for producing both electricity and Domestic Hot Water (DHW). This house has been designed considering sustainability criteria by means of structural and technological measures to ensure energy efficiency. The electric and DHW systems installed in the house are depicted in Fig. 1.

Specifically, the electric power is generated from the following systems:

- **Photovoltaic system.** It has twenty-two polycrystalline silicon photovoltaic modules with a total installed power of 2.7 kW. The panels are located on the roof of the house, distributed in three independent electrical circuits depending on the orientation (East, South and West).
- **Wind turbine system.** A 1.5 kW low-power two-blade wind turbine located in the northeast of the house, on an eight-meter-high tower.
- **Power grid.** It is responsible for supplying electricity in the absence of renewable resources.

For the DHW production, the climatic house has the following systems:

- **Solar thermal system.** Eight panels are located on the south roof of the house, with a total collection area of 20 m^2. The hot water is stored in a 1000 l storage tank.
- **Biomas system.** Located in the boiler room, this allows power regulation from 7 kW to 20 kW. It uses pellets stored in a silo as biofuel.
- **Geothermal system.** The system is made up of five hundred meters of horizontal pipes for the extraction of thermal energy from the ground. The heat pump has a nominal power of 8.2 kW.

2.2. Wind generator

This section provides a detailed description of the wind generation system, where the anomalies must be detected. The main structure of the electricity generation and conditioning is summarized in Fig. 2 and described below.

2.2.1. Power generation

The electricity is generated using a BORNAY INCLIN 1.500 system [22], that has two wind generator blades in charge of converting the wind speed into a rotatory movement. A PMSG neodymium alternator, covered by a carbon fiber housing, takes advantage of its motion to generate electric power. This housing has a rudder in the backside to ensure the proper system orientation. The main features of this system at nominal operation is summarized in Table 1.

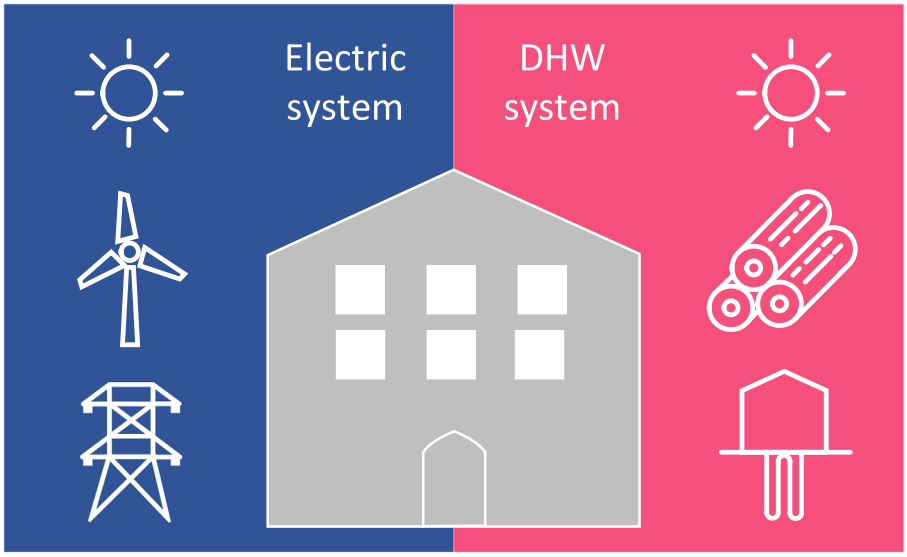

Fig. 1. Electric and DHW system.

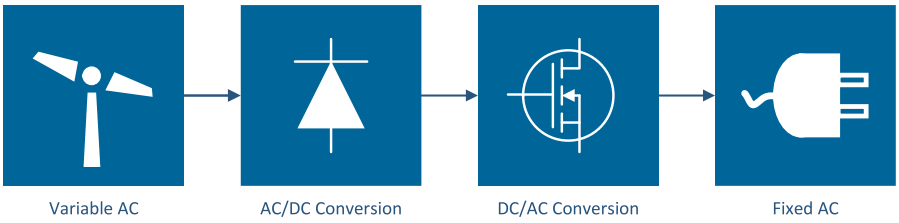

Fig. 2. Energy conversion from turbine to network.

Table 1
Main features of wind generator.

Mechanic features		
Number of blades	Diameter (m)	Material
2	2,86	Carbon fiber
Electric features		
Generator	Power (W)	Voltage (V)
3-ph PMSG	1500	120
Wind features		
Starting speed (m/s)	Nominal power speed (m/s)	Automatic break speed (m/s)
3,5	12	14

Fig. 3 represents the power generated depending on the wind speed. From this figure, it can be concluded that the optimum wind speed is 14 m/s, corresponding to the highest power (1700 W). Furthermore, wind speeds lower than 3 m/s barely leads to power generation.

The rotatory motion of the wind generator produces Alternating Current (AC) electricity with a non-fixed frequency. As the electrical outlet must have a fixed voltage and frequency, a rectifying and inverting stages are necessary.

2.2.2. Rectifying stage

To ensure a fixed frequency, a rectifier stage must be implemented to convert the AC electricity from the alternator into Direct Current (DC). The rectifier uses capacitors, semiconductors and a voltage regulator to establish a fixed DC Voltage (48 V), regardless the input frequency. In this case, The regulator has the possibility of managing a battery system. However, this operation is not considered in the installation.

2.2.3. Inverting stage

Once a constant DC voltage is achieved using the rectifying stage, it is necessary to convert it again to AC with 220 V and 50 Hz, which are the common electric outlet features. To do so, a BORNAY AURORA 3600 inverter [22] is connected to the system. This device consists of two stages, a DC/DC boost converter plus a DC/AC single phase inverter. The main features of this device are summarized in Table 2.

2.3. Total Harmonic Distortion

The rectifier and inverter described in previous subsection are known as power electronics circuits, since they convert AC to DC or DC to AC [17]. One of the key concerns of power electronics systems, is the possibility of converting to active power all the apparent power supplied by a system [17,23]. Considering a power source whose voltage ($v(t)$, in V) and current ($i(t)$, in A) waves are periodic (T), the active power generated (P, in W) can be calculated following Eq. 1.

$$P = \frac{1}{T}\int_{t}^{t+T} v(t)\cdot i(t)dt \tag{1}$$

On the other hand, the apparent power (S, in VA) of this power source can be computed according to Eq. 2.

$$S = V_{rms}\cdot I_{rms} \tag{2}$$

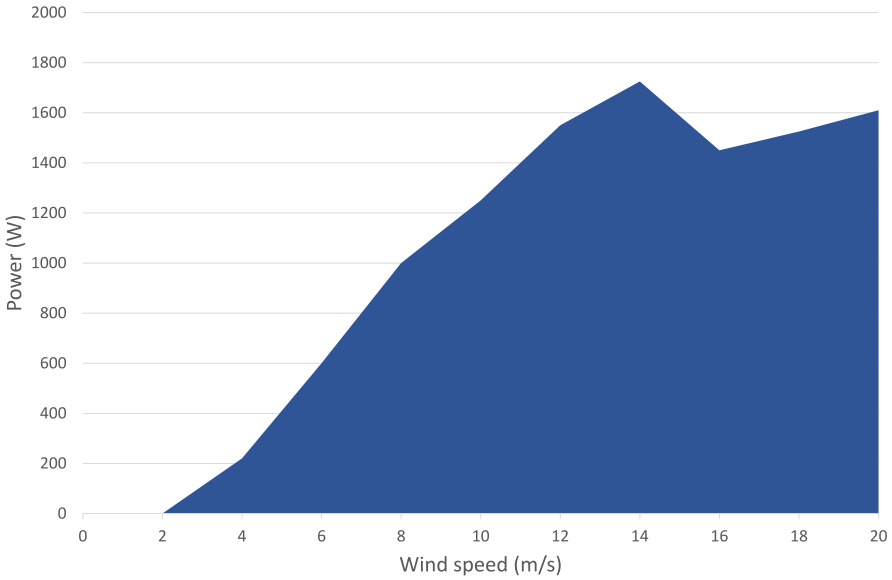

Fig. 3. Relationship between power generated and wind speed.

Table 2
Main features of electric inverter.

Electric Features		
Power (W)	Efficiency (%)	Waveform
3600	96	True sine wave
Output Parameters		
Voltage (V)	Frequency (Hz)	Max.Current (A)
230	50	16

Where *rms* is the Root Mean Square value, that is calculated following Eq. 3.

$$X_{rms} = \sqrt{\frac{1}{T}\int_{t}^{t+T} x^2(t)dt} \tag{3}$$

As stated above, it would be desirable to convert all the apparent power to active power, since it is the power that develops mechanical works [23]. However, the nature of the loads can hinder this objective. Loads that present capacitive or inductive behaviors, produce delays between current and voltage, which leads to reduce the active power, even though the apparent power is the same [17]. This part of the apparent power, used to create electric and magnetic fields, is known as reactive power (*Q*, in VAr) [23]. Fig. 4 represents the influence of delays between voltage and currents through two examples. The left chart presents a voltage (blue line) and a current (red line) with the same phase. The active power is the result of integrating the instantaneous power (black line). In this case, it is always positive. However, in the right chart, the delay between voltage and current results in some negative instantaneous power. This means that the active power in this case is lower, although V_{rms} and *Irms* have the same value in both graphs.

Apart from the inductive and capacitive loads, the use of semiconductors caused loads that present a non-linear behavior, since their operating mode change during one period [17]. Then, in power electronic circuits, the typical sinus waves can be converted to non-sinus periodical waves. Eq. 4 presents how a periodical non-sinus wave $x(t)$ can be presented as a sum of sinus whose frequencies are multiple of the original, following the Fourier transform [24].

$$x(t) = X_0 + \sum_{n=1}^{\infty} X_n \cdot sin(n\omega t + \phi_n) \tag{4}$$

Lets suppose a sinus voltage source that is connected to a non-linear load, producing a non-linear current, whose Fourier Transforms are presented in Fig. 5. In this case, the active power is com-

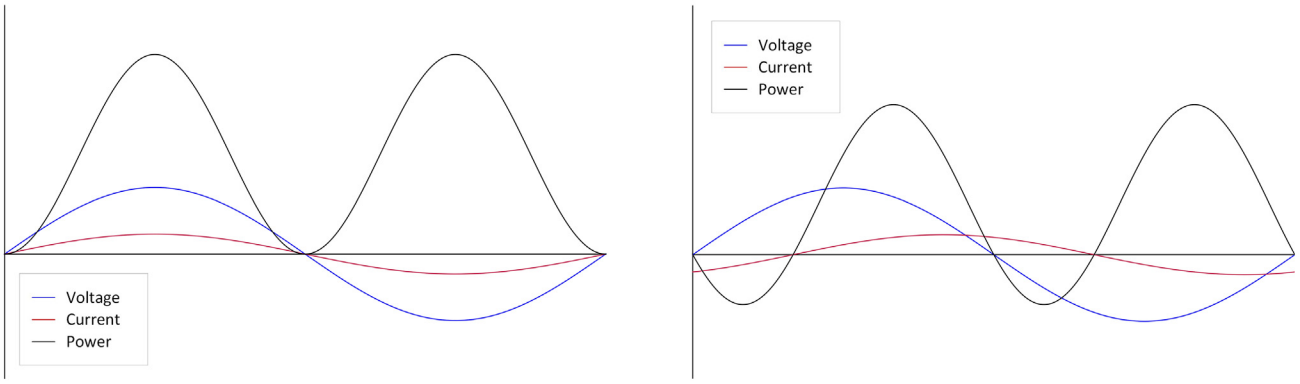

Fig. 4. Influence of voltage and current phase on the active power.

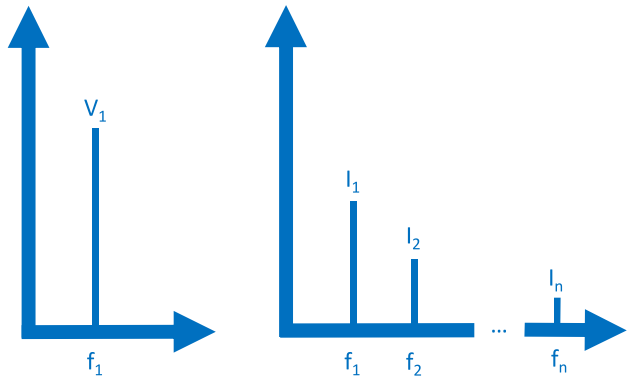

Fig. 5. Fourier Transform of Voltage and Current.

puted according to Eq. 5. For this example only the voltage and current with $n = 1$ generates real power, but the apparent power takes into consideration all current harmonics.

$$P = \frac{1}{T}\sum_{n=1}^{\infty}\int_{t}^{t+T} V_n sin(n\omega t)\cdot I_n sin(n\omega t + \phi_n)dt = P_1 \tag{5}$$

This example emphasizes how important is to avoid the harmonics occurrence in power electronics circuits, such as rectifiers and inverters. To monitor the performance of a power electronic circuit, different parameters are measured, being especially important the Power Pactor (*PF*) and the Total Harmonic Distortion (*THD*) shown in Eq. 6 [23].

$$PF = \frac{P}{S} \qquad THD = \sqrt{\frac{\sum_{n\neq 1}^{\infty} I_n^2}{I_1^2}} \tag{6}$$

The *PF* determines the fraction of apparent power is converted to real power, and it is directly related to the harmonic appearance, as shown in the previous example. The *THD* coefficient establishes a relationship between the first harmonic (the one with the fundamental frequency) and the rest of harmonics, that do not contribute to the real power *P*. Hence, a proper power electronic circuit must present high *PF* and low *THD* [17,23].

2.4. Dataset description

To implement an anomaly detection system capable of detecting malfunction in power electronic devices, the following parameters are monitored with a sample rate of 10 min.

- **Electric parameters.**
  - Voltage (V_{rms}) supplied by the inverter.
  - Current (I_{rms}) supplied by the inverter.
  - Active power (P) generated.
  - Reactive power (Q) generated.
- **Meteorological parameters.**
  - Wind speed (m/s).
  - Wind direction (°).
  - Wind direction at 10 m (°).
  - Atmospheric pressure ($mbar$).
  - Temperature (° C).

The initial dataset included the measurements of these 9 variables during the normal operation from April to July, both included. After samples removing with null power generated, the used dataset is comprised of 16540 samples.

3. One-class classification techniques

The different one-class techniques used to model the target set to achieve the one-class classifiers are detailed in this section.

3.1. Approximate Polytope Ensemble

As stated in the introduction section, a very common way to model the training set consists of determining its geometric boundaries [25]. In this sense, the convex hull calculation can be presented as very interesting tool to model the limits. By definition, the convex hull *CH* of a given training set $\boldsymbol{X}\subset \mathbb{R}^n$ is the minimal convex set containing $\boldsymbol{X}$ following the Eq. 7 [26,27].

$$CH(X) = \left\{\sum_{i=1}^{N}\beta_i \boldsymbol{x_i} \| \sum_{i=1}^{N}\beta_i = 1, 0 \leqslant \beta_i \leqslant 1\right\} \tag{7}$$

Where:

- N is the number of objects of the training set $\boldsymbol{X}$.
- β_i is the coefficient of $\boldsymbol{x_i}$.

This approach has the possibility of expanding or contracting the vertexes $\boldsymbol{v}$ from the a centroid $\boldsymbol{c}$, using a parameter θ according to 8.

$$\boldsymbol{v}^{\theta} : \{\theta \boldsymbol{v} + (1-\theta)\boldsymbol{c} | \boldsymbol{v} \in CH(\boldsymbol{X})\} \tag{8}$$

The parameter $\theta \in [0, +\infty)$would expand the hull with values greater than 1, and contract it with values lower than 1.

This method has proven to be effective, however its computational cost is significantly high, especially with high-dimensional datasets [25]. Then, the Approximate Polytope Ensemble (APE) method proposes a simplification of this problem by means of performing π random 2D projections over the original dataset. Then, for each plane π_i the convex hull is computed, resulting in a reduction in the computational needs.

Once the convex hulls of the π projections are calculated, the data test is labeled as anomalous if it is outside of at least one convex hull projection [25]. APE also has the possibility of using the parameter θ to contract or expand the decision boundary over each projection.

3.2. Support vector data description

The Support Vector Data Description (SVDD) is another boundary method, developed from the well-known Support Vector Machine (SVM). SVM has been used for both regression and classification problems [28]. In one-class classification, the main basis of SVM is to project the training objects into a higher-dimensional feature space and then, an hyper-plane that maximises the distance to the origin is constructed [29].

Using this general idea, the SVDD algorithm aims to implement a hyper-sphere of radius $\boldsymbol{R}$ to enclosed the training data, which represents the target set [30]. Hence, the training stage consists of determining the minimum hyper-sphere with center $\boldsymbol{c}$, and radius $\boldsymbol{R}$ through Eq. 9, subjected to the constraints in Eq. 10 [31].

$$F(\boldsymbol{R}, \boldsymbol{c}, \boldsymbol{\alpha_i}) = \boldsymbol{R}^2 + T\sum_{i}\boldsymbol{\alpha_i} \tag{9}$$

$$||\boldsymbol{x_i} - \boldsymbol{c}||^2 \leqslant \boldsymbol{R}^2 + \boldsymbol{\alpha_i} \qquad \boldsymbol{\alpha_i} \leqslant \boldsymbol{R}^2 \tag{10}$$

where:

- α_i is the slack variable.
- T is a trade-off parameter that relates the volume and the errors in the training set.

The mentioned trade-off allows the possibility of having anomalous objects in the target set. The procedure to determine the anomaly consists of calculating of the test data belongs to the hyper-sphere or not. The use of SVDD has been successfully applied to solve one-class problems in many different fields [18].

3.3. Autoencoder artificial neural network

Focusing on dimensional reduction methods, the use of Artificial Neural Networks (ANN) with an Autoencoder configuration has led to significant good results [21].

One of the most typical ANN architectures, the Multilayer Perceptron (MLP) [32], is used with this aim. This topology is divided into three parts or layers, formed by neurons. The input layer, the hidden layer and the output layer. The output of the hidden layer is calculated following Eq. 11.

$$\boldsymbol{h_l} = f_{HL}(\boldsymbol{W_{HLx}} + \boldsymbol{p_{HL}}) \tag{11}$$

where:

- $\boldsymbol{h_l}$ is the output of the hidden layer.
- $\boldsymbol{f_{HL}}$ is activation function of the hidden layer.
- $\boldsymbol{W_{HL}}$ is Weight matrix between input and hidden layers.
- $\boldsymbol{p_{HL}}$ is the bias vector.

Consequently, the output of the ANN is computed according to 12.

$$\hat{\boldsymbol{x}} = f_o(\boldsymbol{W_o h_l} + \boldsymbol{p_o}) \tag{12}$$

where:

- $\hat{\boldsymbol{x}}$ is the output of the ANN.
- $\boldsymbol{f_o}$ is activation function of the output layer.
- $\boldsymbol{W_o}$ is Weight matrix between hidden and output layers.
- $\boldsymbol{p_o}$ is the bias vector.

The main basis of Autoencoder consists of training an ANN whose output $\hat{\boldsymbol{x}}$ must be the same as the input $\boldsymbol{x}$. In addition, a non-linear reduction must be carried out in the hidden layer through the activation function. This means that, the number of neurons in the hidden layer must be less than the number of inputs. Hence, a decompression is implemented at the output [21]. The Autoencoder technique is based on the premise that anomalous points would be significantly different than normal points in the hidden layer subspace. Then, the decompression would lead to high reconstruction error [21].

3.4. Principal component analysis

The Principal Component Analysis (PCA) technique, has been applied to solve data dimensionality reduction problems. The objective of reducing dimensions with the minimum loss of information is met by calculating the directions with higher variability [33].

This main directions, known as components are computed through the eigenvectors calculated from the eigenvalues of the covariance matrix. By means of these eigeinvectors, PCA establishes new variables by projecting the original points into the eigeinvectors subspace. As this technique implies linear transformations, its use leads to especially good results when it is applied to clearly linear subspace [18].

Although the good performance in dimensional reduction tasks, PCA can also be applied in one-class problems using the reconstruction error criteria. Lets imagine a training set $\boldsymbol{X} \in \mathbb{R}^2$. Using one of the two principal components, it can be linearly transformed into $\widehat{\boldsymbol{X}} \in \mathbb{R}^1$. Then a test data $\boldsymbol{x_t}$ is labeled following a reconstruction error criteria (Eq. 13). This error is calculated as the difference between the initial point $\boldsymbol{x_t}$ and its projection $\hat{\boldsymbol{x}}_{\boldsymbol{t}}$.

Since anomalous points should imply great reconstruction errors, when the reconstruction error of a test data is above a specific threshold, the anomaly is detected.

$$e(x) = ||\boldsymbol{x_t} - \hat{\boldsymbol{x}}_{\boldsymbol{t}}|| \tag{13}$$

3.5. k-nearest neighbor

The k-Nearest Neighbor (kNN) technique bases the novelty detection on the distances between target and test objects. Its use for one-class has shown interesting performance in a wide variety of UCI repository datasets [34].

In this case, the anomalous behavior of a given point $\boldsymbol{x} \in \mathbb{R}^n$, is estimated depending on the local density of the hyper-sphere containing its k^{th} nearest neighbors [28]. More specifically, $\boldsymbol{x}$ would be labeled as anomalous if the distance to the k^{th} nearest neighbor belonging to the training data ($kNN^{tr}(\boldsymbol{x})$) is greater than the local distance from the k^{th} neighbor to its k^{th} neighbor [18].

$$d(\boldsymbol{x}) = \frac{\left|\left|\boldsymbol{x} - kNN^{tr}(\boldsymbol{x})\right|\right|}{\left|\left|kNN^{tr}(\boldsymbol{x}) - kNN^{tr}\left(kNN^{tr}(\boldsymbol{x})\right)\right|\right|} \tag{14}$$

The value of k has a significant importance, since an increase could imply a loss in the noise sensitivity, but the local sensitivity would decrease [18]. It is important to remark that the proper value of k depends on the dataset shape and distribution [28].

3.6. Gaussian classifier

This density estimation methods is, due to its simplicity and good performance, one of the most used one-class classification technique. It is based on the idea that the target set follows a Gaussian or normal distribution. Then, non-target instances during the test phased would not fit the training model.

Lets suppose a test instance $x \in \mathbb{R}^n$, whose probability distribution function is described in Eq. 15 [18]. If x does not belong to the target class, the function would return lower values. Then, a proper threshold would lead to a proper classification.

$$p(x, \mu, \Sigma) = \frac{1}{(2\pi)^{n/2}|\Sigma|^{1/2}} e^{-\frac{1}{2}(x-\mu)^T \Sigma^{-1}(x-\mu)} \tag{15}$$

where:

- μ – Mean value of the training set.
- Σ – Covariance matrix of the training set.

One of the strengths of this method, is the low computational effort [18], being the covariance matrix calculation the hardest step. The possibility of applying a regularization parameter R_p may result a useful tool, especially when the inverse of covariance can not be calculated.

This method presents good performance, especially if the target set has a normal shape [35]. One of its limitations, that is shared with other density estimation methods, is the need of a significantly high training dataset [36].

4. Experiments and results

The present section describes the different achieved experiments to evaluate the performance of the described techniques.

4.1. Anomaly generation

Since the dataset is comprised of data from correct system operation, it is necessary to have a testing set with anomalies. Taking into consideration that the anomalies could be the consequence of wrong power electronics circuits operation, three different kind of electric anomalies are generated:

- Increasing ($p\%$) the measured current I_{rms} with the same P and Q, which means a greater THD.
- Reducing ($p\%$) the real generated power P, with the same I_{rms} and Q, which means a PF reduction.
- Reducting ($p\%$) the reactive power Q, with the same I_{rms} and P, which means a THD increment.

In this case, different values of p will be tested. For all these kind of anomalies, the rest of variables remain unchanged, since they are not related to the good circuit operation. The anomaly generation type applied is randomly selected for each sample. An example of how three test samples are converted into anomalies is shown in Fig. 6.

4.2. Experiments setup

This section details the experiments carried out to evaluate the performance of each technique on the anomaly detection task. For each technique, different hyper-parameters were swept in order to achieve the optimum results.

The generated anomalies correspond to a 20% of the initial dataset. The modification percentage p is varied from 10 to 90% with a 10% step. Then, each technique is assessed 9 times, one for each variation p. This assessment has been carried out using the Area Under the Receiver Operating Characteristic Curve (AUC) [37]. The AUC (%) has offered a really interesting performance, with the particular feature of being insensitive to changes in class distribution, which is a key factor in one-class classification tasks [38].

To ensure a proper analysis, a $k-fold$ cross-validation method was implemented with $k=10$. An example of how this method works with $k=3$ is depicted in Fig. 7, where the tartet set is divided into three subgroups $T1, T2$ and $T3$.

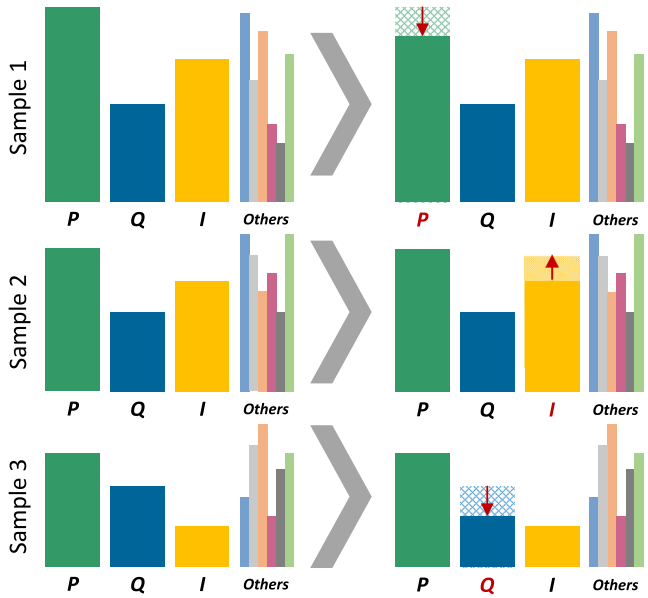

Fig. 6. Example of anomaly generation.

Also, different data conditioning was tested: a 0 to 1 normalization and a ZScore normalization. Let suppose a dataset whose mean (μ) and standard deviation (σ) are calculated. For a point x, ZScore measures how many standard deviations is a sample is away from the mean [39]. Also, the time needed to train each classifier $t_c(s)$ was registered and used as measure of the computational cost of each technique. The time to label the test data is not represented, since it is always far below the sample time, which is 10 min.

4.3. Results

A detailed analysis of the results offered by each technique is presented in the following subsections.

4.3.1. APE results

The results for APE (Table 3 and Fig. 8) shows that this technique is not able to classify the anomalies when the outliers are generated with low percentage variations. However, with more than 60% of variation, this technique shows an increasing performance. Although the 0 to 1 and Zscore normalizations were tested, the best results were always achieved without applying a data conditioning. The proper number of projections π is always 1000, except with a 10% of variation, whose performance is always a 50% AUC. The t_c is lower than most techniques, however it is not the lowest.

4.3.2. SVDD results

The SVDD results presented in Table 4 and Fig. 9 present a remarkable high t_c. However, for this application, this is not an important problem because the data is registered with a 10 min sample rate. As it happened with APE, the performance tendency increases with the percentage of variation of the generated outliers. However, AUC values are always below 90%. The outlier percentage in the training set (TrO) is reduced as the variation increases. This parameter establishes the fraction of training data considered as anomalous. This situation is produced because the outliers generated with low percentage variation are very similar to some training instances. Finally, all best classifiers were obtained trough a Zscore conditioning.

4.3.3. Autoencoder results

The Autoencoder classifiers have always the best AUC results when they apply a low dimensional reduction in the hidden layer, with a proper configuration of Neurons in the Hidden Layer (NHL) of 8 or 7 (Table 5 and Fig. 10). It is important to remark that acceptable values of AUC are reached for 30% of measurement variation. As for SVDD, the TrO increases with the outlier variation tested. In

Fig. 7. Example of anomaly generation.

Table 3
Best APE classifier for each ourlier variation.

Var. (%)	Condit.	π	AUC (%)	$t_c(s)$
10	NA	5	50,000	0,002
20	NA	1000	50,256	0,263
30	NA	1000	51,346	0,330
40	NA	1000	60,844	0,465
50	NA	1000	69,478	0,338
60	NA	1000	81,066	0,316
70	NA	1000	87,899	0,344
80	NA	1000	93,385	0,366
90	NA	1000	96,330	0,371

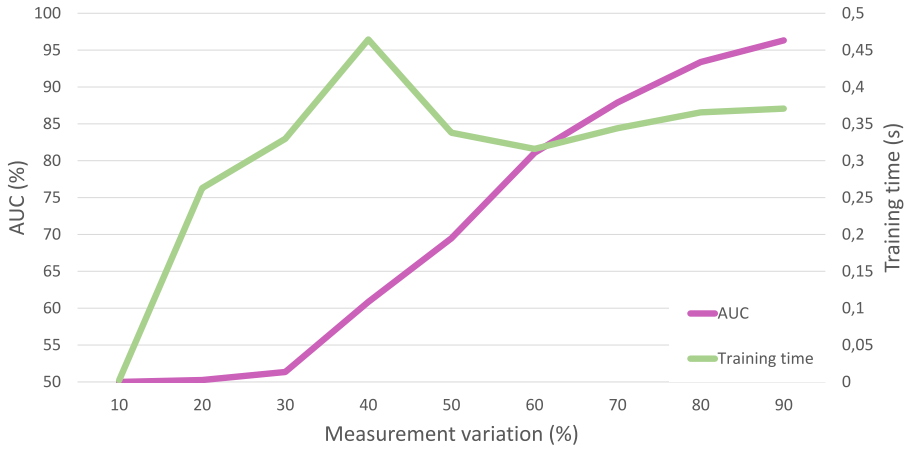

Fig. 8. General results for APE technique.

Table 4
Best SVDD classifier for each ourlier variation.

Variation (%)	Norm	Outlier (%)	AUC (%)	$t_c(s)$
10	Zscore	20	53,364	23,428
20	Zscore	30	58,260	23,622
30	Zscore	30	61,612	23,558
40	Zscore	0	73,056	27,824
50	Zscore	0	82,407	24,176
60	Zscore	0	86,328	24,664
70	Zscore	0	88,663	24,293
80	Zscore	0	88,783	24,442
90	Zscore	0	89,103	25,570

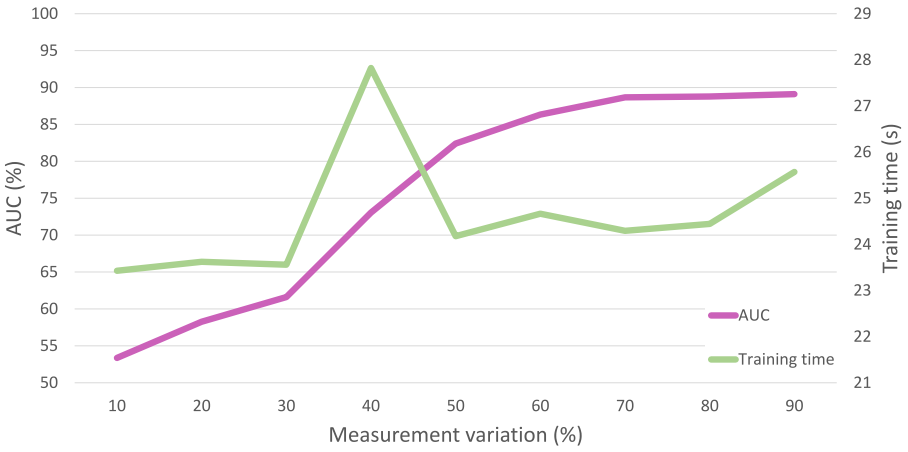

Fig. 9. General results for SVDD technique.

Table 5
Best Autoencoder classifier for each outlier variation.

Var. (%)	Condit.	NHL	TrO (%)	AUC (%)	$t_c(s)$
10	Zscore	8	20	57,283	2,330
20	Zscore	8	30	63,775	2,076
30	Zscore	8	30	75,311	3,095
40	Zscore	8	20	83,969	3,263
50	Zscore	8	10	87,248	3,123
60	Zscore	8	10	91,986	2,617
70	0 to 1	8	10	93,428	3,634
80	Zscore	7	10	94,307	2,264
90	Zscore	8	10	94,727	2,825

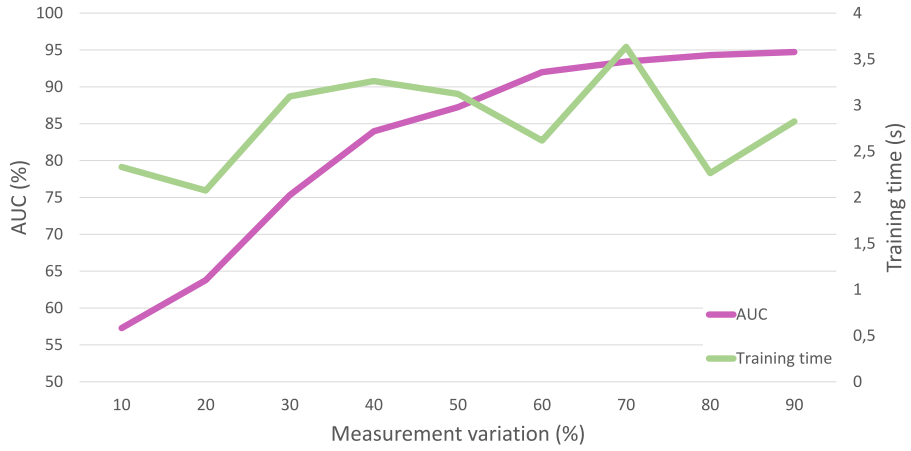

Fig. 10. General results for Autoencoder technique.

Table 6
Best PCA classifier for each outlier variation.

Var. (%)	Condit.	Component	TrO (%)	AUC (%)	$t_c(s)$
10	Zscore	8	30	59,195	0,026
20	NA	8	20	72,825	0,022
30	0 to 1	8	20	79,286	0,022
40	NA	8	10	85,580	0,033
50	0 to 1	8	10	84,091	0,026
60	0 to 1	6	10	90,030	0,022
70	0 to 1	7	10	92,838	0,025
80	Zscore	6	10	94,085	0,028
90	0 to 1	7	0	97,745	0,025

the majority of cases, the Zscore is the best conditiong process. Regarding the computation time, this is the second slowest technique.

4.3.4. PCA results

Like in the Autoencoder case, this reconstruction technique achieves its best results with low dimensional reduction (Table 6 and Fig. 11). The performance of PCA is very similar to the Autoencoder regarding the TrO value, also produced by the same reasons. This technique presents a significantly low computation time with values below 34 ms. Furthermore, the AUC with a 30% of variation almost reaches the 80%, which represents a really interesting achievement.

4.3.5. kNN results

From Table 7 and Fig. 12, it can be derived that the parameter kNN, that determines the number of neighbors taken into account to achieve the classifier, is always 1 or 2. The same trend as for SVDD, Autoencoder and PCA has been detected regarding the outlier fraction of the training set (TrO). Training times are slightly greater than the ones obtained with APE. The AUC values are significantly good from a 40% to 90% variation.

4.3.6. Gaussian results

The results obtained using Gaussian classifiers (Table 8 and Fig. 13), show some important points. First, it is presented as the fastest technique, with training times below 9 ms in the worst case. It is also important to remark that, once it is exceeded the 30% of variation, this classifier performs in a successful way. In this case, the TrO follows a declining trend with the percentage variation, although it is not as significant as in other techniques.

5. Discussion

After the deep analysis carried out in the Results section, some of the main findings of this research work are discussed. First, PCA method has shown a good average performance, being between the top three classifiers for all tests. It is the leading method when

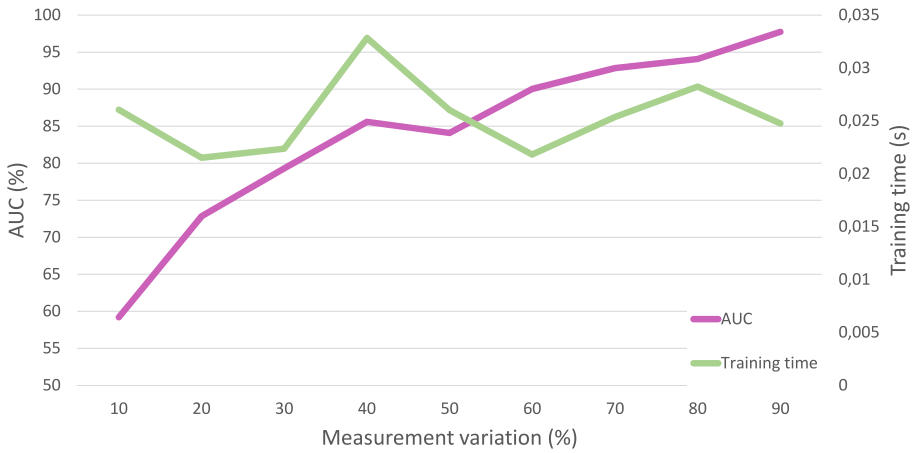

Fig. 11. General results for PCA technique.

Table 7
Best kNN classifier for each outlier variation.

Var. (%)	Condit.	kNN	TrO (%)	AUC (%)	$t_c(s)$
10	0 to1	1	30	56,716	0,525
20	0 to1	1	30	65,629	0,332
30	0 to1	1	30	68,537	0,333
40	Zscore	1	20	79,035	0,416
50	Zscore	1	10	85,354	0,365
60	Zscore	1	10	88,586	0,347
70	Zscore	1	10	90,995	0,353
80	Zscore	1	10	91,822	0,356
90	NA	2	10	93,255	0,373

the harmonic distortion presents low variation (10% to 40%), and also when the greatest distortion is introduced (90%). It is also worth noting that, in spite of the good results, it is the technique with the second lowest training time.

At this point, it is important to remark the good performance of Gaussian classifier that delivered good results when the outlier deviation is above 40%. Furthermore, it is the fastest technique in terms of computation time. However, it presents the significant weakness of poor performance when applied over low harmonic distortion deviations. The rest of techniques presented a similar trend but with lower AUC results and greater training times, being significantly high the t_c values of SVDD.

For those techniques where the TrO were tested, an interesting finding is reached. An increment in the variation leads to a decrement in the TrO. This is produced because at low percentage variations, the target set and the non-target set presents significant similarities. In this situation, it is necessary to increment the threshold to determine anomalous instances, which is represented by TrO.

Finally, there is not a clear trend about the best data conditioning. It presents a different behavior depending on the technique applied.

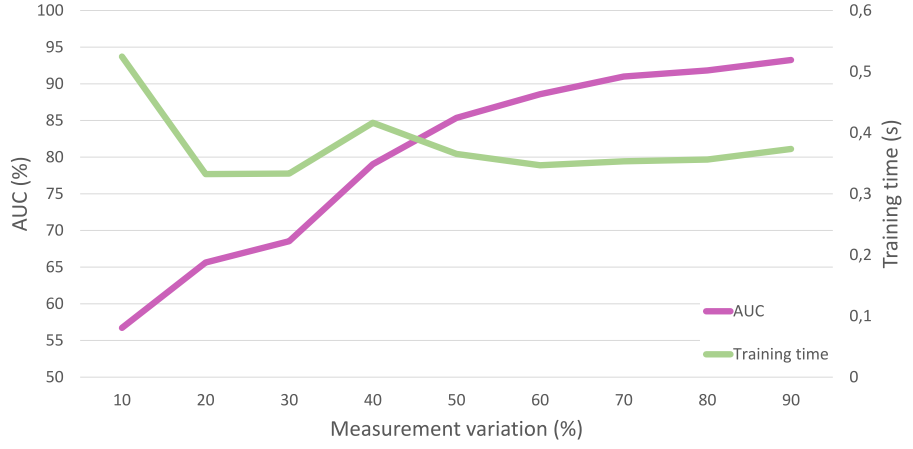

Fig. 12. General results for kNN technique.

Table 8
Best Gaussian classifier for each outlier variation.

Var. (%)	Condit.	TrO (%)	AUC (%)	$t_c(s)$
10	0 to1	10	52,833	0,008
20	Zscore	15	57,856	0,004
30	0 to1	15	66,911	0,009
40	Zscore	15	83,304	0,004
50	NA	10	89,712	0,008
60	NA	5	93,106	0,004
70	Zscore	5	95,004	0,004
80	Zscore	5	95,872	0,004
90	Zscore	5	96,504	0,004

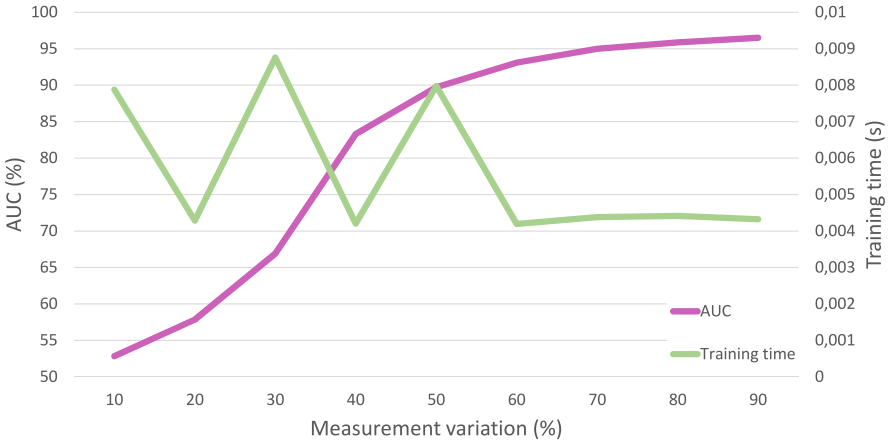

Fig. 13. General results for Gauss technique.

6. Conclusions and future works

The renewable energy field is being promoted as a key piece for a sustainable growth in next generations. In this context, the wind energy presents an important share of this opportunity. Then, this work has proposed and analysed the use of six different one-class techniques to detect malfunctions in wind generator circuits placed in a bioclimatic house, whose aim is the energy efficiency increasing and maintenance reduction of this part. From an initial dataset, corresponding to meteorologic and electric variables, and obtained during the correct operation, different classifiers were implemented.

These classifiers were tested and assessed through artificially generated anomalies that emulate electric distortions derived from power electronic circuits failures. These anomalies consisted on modifying a given percentage one electric variable randomly selected (I_{rms}, P, Q).

In general terms, the implemented classifiers has shown successful performance in the anomaly detection tasks, as detailed in the results.

Since the electronic circuits used in this kind of installations are subjected to an intense maintenance plan, the proposed approach could be physically implemented in the installation as a key step to reduce predictive and corrective maintenance costs. Other significant improvement is the fact that quality parameters of the resulting electric energy would be ensured.

In future works, it could be considered the idea of reducing the sample rate, because, in the worst case scenario, an anomaly would be detected 10 late. Then, reducing the sample rate would reduce the reaction time.

Focusing on the anomalies used to test the classifier, two possible ways can be considered. First, it would be interesting to analyze each technique with other kind of artificially generated anomalies, such as noise or distortion. On the other hand, the possibility of forcing the circuits to typical real malfunctions could represent a good tool to validate the proposed method.

Furthermore, the classifier implementation could include, in future works, two additional features. First, the possibility of retrain the system online as it is working could be considered. Finally, as different operating points can be presented in the wind turbine, a prior clustering stage could be an interesting starting point before implementing a hybrid one-class topology.

CRediT authorship contribution statement

Esteban Jove: Conceptualization, Methodology. **Jose Manuel González-Cava:** Resources. **José-Luis Casteleiro-Roca:** Software. **Héctor Alaiz-Moretón:** Writing - original draft. **Bruno Baruque:** Data curation. **Paulo Leitão:** Formal analysis. **Juan Albino Méndez Pérez:** Visualization, Writing - review & editing. **José Luis Calvo-Rolle:** Writing - review & editing, Supervision, Project administration.

Declaration of Competing Interest

The authors declare that they have no known competing financial interests or personal relationships that could have appeared to influence the work reported in this paper.

Acknowledgements

This study was supported by CajaCanarias Foundation with the project PR705752 (GreenTourist, 2016TUR17).

Jose M. Gonzalez-Cava's research was supported by the Spanish Ministry of Science, Innovation and Universities (www.ciencia.gob.es) under the "Formación de Profesorado Universitario" grant FPU15/03347.

References

[1] Government of Spain, Real decreto-ley 15/2018, de 5 de octubre, de medidas urgentes para la transición energética y la protección de los consumidores., 2018. BOE-A-2018-13593. .
[2] X. Simón, D. Copena, Eolic energy and rural development: an analysis for galicia, Spanish J. Rural Dev. 3 (2012).
[3] Repsol's Economic Research Department, Ann. Energy-statistics (2019) 2019.
[4] P.A. Owusu, S. Asumadu-Sarkodie, A review of renewable energy sources, sustainability issues and climate change mitigation, Cogent Eng. 3 (2016) 1167990.
[5] H. Lund, Renewable energy strategies for sustainable development, Energy 32 (2007) 912–919.
[6] Asociación Empresarial Eólica (AEE), Anuario eólico. la voz del sector 2019, 2019. .
[7] P. Sorknæs, S.R. Djørup, H. Lund, J.Z. Thellufsen, Quantifying the influence of wind power and photovoltaic on future electricity market prices, Energy Conversion Manage. 180 (2019) 312–324.
[8] D. Infield, L. Freris, Renewable energy in power systems, John Wiley & Sons, 2020.
[9] British Petroleum, Renewable energy - wind energy, 2018. .
[10] Informe sobre los elementos necesarios en la transición energética, https://www.aeeolica.org/uploads/Elementos_necesarios_para_la_Transicin_Energtica_FINAL.pdf, 2017. Accessed: 2020-05-21. .
[11] Y. Kumar, J. Ringenberg, S.S. Depuru, V.K. Devabhaktuni, J.W. Lee, E. Nikolaidis, B. Andersen, A. Afjeh, Wind energy: Trends and enabling technologies, Renew. Sustain. Energy Rev. 53 (2016) 209–224.
[12] I. Paraschivoiu, S. Ammar, F. Saeed, VAWT versus HAWT: A comparative performance study of 2–6 MW rated capacity turbines, Trans. Canadian Society Mech. Eng. (2018).
[13] S. Bhatia, Advanced Renewable Energy Systems, Woodhead Publishing India, 2014.
[14] A.D. Hansen, G. Michalke, Fault ride-through capability of dfig wind turbines, Renewable Energy 32 (2007) 1594–1610.
[15] P. Gajewski, K. Pieńkowski, Advanced control of direct-driven pmsg generator in wind turbine system, Arch. Electr. Eng. 65 (2016) 643–656.
[16] I. Parmee, P. Hajela, Optimization in industry, Springer Science & Business Media, 2012.
[17] D.W. Hart, Power electronics, Tata McGraw-Hill Education, 2011.
[18] D.M.J. Tax, One-class classification: concept-learning in the absence of counter-examples [ph d. thesis], Delft University of Technology, 2001.
[19] V. Chandola, A. Banerjee, V. Kumar, Anomaly detection: A survey, ACM Computing Surveys (CSUR) 41 (2009) 15.
[20] P. Casale, O. Pujol, P. Radeva, Approximate convex hulls family for one-class classification, in: International Workshop on Multiple Classifier Systems, Springer, pp. 106–115. .
[21] M. Sakurada, T. Yairi, Anomaly detection using autoencoders with nonlinear dimensionality reduction, in: Proceedings of the MLSDA 2014 2nd Workshop on Machine Learning for Sensory Data Analysis, ACM, p. 4. .
[22] Sotavento installation, http://web.archive.org/web/20080207010024/http://www.808multimedia.com/winnt/kernel.htm, 2020. Accessed: 2020-03-19. .
[23] M.H. Rashid, Power electronics handbook: devices, circuits and applications, Elsevier, 2010.
[24] I.N. Sneddon, Fourier transforms, Courier Corporation (1995).
[25] D. Fernández-Francos, ó. Fontenla-Romero, A. Alonso-Betanzos, One-class convex hull-based algorithm for classification in distributed environments, IEEE Transactions on Systems, Man, and Cybernetics: Systems (2018) 1–11. .
[26] M. Zeng, Y. Yang, S. Luo, J. Cheng, One-class classification based on the convex hull for bearing fault detection, Mech. Systems Signal Processing 81 (2016) 274–293.
[27] F.P. Preparata, M.I. Shamos, Computational geometry: an introduction, Springer Science & Business Media, 2012.
[28] T. Sukchotrat, Data mining-driven approahces for process monitoring and diagnosis, Ind. Manuf. Eng. (2009).
[29] P. Rebentrost, M. Mohseni, S. Lloyd, Quantum support vector machine for big data classification, Phys. Rev. Lett. 113 (2014) 130503.
[30] C. Sanchez-Hernandez, D.S. Boyd, G.M. Foody, One-class classification for mapping a specific land-cover class: Svdd classification of fenland, IEEE Trans. Geosci. Remote Sens. 45 (2007) 1061–1073.
[31] J.H. Shin, B. Lee, K.S. Park, Detection of abnormal living patterns for elderly living alone using support vector data description, IEEE Trans. Inf Technol. Biomed. 15 (2011) 438–448.
[32] E. Jove, J.M. Gonzalez-Cava, J.-L. Casteleiro-Roca, J.-A. Méndez-Pérez, J. Antonio Reboso-Morales, F. Javier Pérez-Castelo, F. Javier de Cos Juez, J. Luis Calvo-Rolle, Modelling the hypnotic patient response in general anaesthesia using intelligent models, Logic Journal of the IGPL (2018). .
[33] M. Ringnér, What is principal component analysis?, Nature Biotechnol 26 (2008) 303.
[34] P. Casale, O. Pujol, P. Radeva, Approximate convex hulls family for one-class classification, in: C. Sansone, J. Kittler, F. Roli (Eds.), Multiple Classifier Systems, Springer, Berlin Heidelberg, Berlin, Heidelberg, 2011, pp. 106–115.
[35] P. Casale, O. Pujol, P. Radeva, Approximate polytope ensemble for one-class classification, Pattern Recogn. 47 (2014) 854–864.
[36] B. Jeon, D.A. Landgrebe, Fast parzen density estimation using clustering-based branch and bound, IEEE Trans. Pattern Anal. Mach. Intell. 16 (1994) 950–954.
[37] A.P. Bradley, The use of the area under the roc curve in the evaluation of machine learning algorithms, Pattern Recogn. 30 (1997) 1145–1159.
[38] T. Fawcett, An introduction to roc analysis, Pattern Recogn. Letters 27 (2006) 861–874.
[39] L.A. Shalabi, Z. Shaaban, Normalization as a preprocessing engine for data mining and the approach of preference matrix, in: 2006 International Conference on Dependability of Computer Systems, pp. 207–214. .

Esteban Jove received M.S. degree in Industrial Engineering from the University of Leon in 2014. After two years working in the automotive industry, he joined the University of A Coruña, Spain, where he is Professor of in the Energy Efficiency Master's Degree since 2016. In 2020, he receives the Ph.D in the Industrial, Environmental and Computer Science engineering program, in the University of La Laguna.
His main research interests have been focused on the application of intelligent techniques to model, optimize and detect anomalies in industrial and energetic systems.

José Manuel Gonza'alez Cava was born in 1992. He received his B. Sc in Industrial Electronics and Automatic Control Engineering and M. Sc. In Industrial Engineering from Universidad de La Laguna. He is currently doing a PhD under a "Formación de Profesorado Universitario (FPU)" national fellowship at the Departamento de Ingeniería Informática y de Sistemas. His research interests lie in the application of control theory to the biomedical and the industrial fields. Specifically, he is interested in the control of the anesthetic process.

José Luis Casteleiro Roca has received M.S. and Ph.D. degrees in Industrial Engineering from the University of Leon in 2004 and 2007, respectively. He is an Associate Professor of Automatic Control and the head of the Industrial Engineering Department, Faculty of Engineering, University of A Coruña, Spain. His main research areas are related with the application of expert system technologies in diagnosis and control systems and in intelligent training systems for control engineering, systems optimization and education.

Héctor Alaiz Moretón received his degree in Computer Science, performing the final project at Dublin Institute of Technology, in 2003. He received his Ph.D. in Information Technologies in 2008 (University of Leon). He has worked like a lecturer since 2005 at the School of Engineering at the University of Leon. His research interests include knowledge engineering, machine and deep learning, network communication and security. He has several works published in international conferences, as well as books and scientific papers in peer review journals. He has been a member of scientific committees in conferences. He has headed several Ph.D. Thesis and research projects.

Bruno Baruque Zanón holds an associate professor position at the University of Burgos, Spain since 2018. He obtained his Ph.D. degree in Computer Science/ Artificial Intelligence (with European Mention) in 2009 and his Master Degree in Computer Science in 2004, both at the Univ. of Burgos. He is an active member of the GICAP (Univ. of Burgos) and BISITE (Univ. of Salamanca) research groups. His research interests are focused on the data analysis and automated learning field, with special emphasis in artificial neural networks. He collaborates as guest editor and reviewer of several international journals and as programme committee member in numerous international conferences related with the knowledge area of artificial intelligence.

Paulo Leitao received the MSc and PhD degrees in Electrical and Computer Engineering, both from the University of Porto, Portugal, in 1997 and 2004, respectively. From 1993 to 1999 he developed research activities at the CIM Centre of Porto, and from 1999 to 2000 at Institute for Development and Innovation in Technology (IDIT), Santa Maria da Feira, Portugal. He joined the Polytechnic Institute of Bragan?a, School of Technology and Management, Portugal, in 1995, and currently he is Full Professor in the Department of Electrical Engineering of that institute and coordinator of Center in Digitalization and Intelligent Robotics (CEDRI). His research interests are in the field of intelligent production systems, agent-based and holonic control, re-configurable factory automation, collaborative production automation and high-level Petri nets.

Juan Albino Méndez Pérez is full professor at the University of La Laguna since 1993 in the Department of Computer Science and Systems Engineering. His teaching activity has been focused on system modelling and control. He works on lines of research related to control engineering: fuzzy control, predictive control and control applications. He earned a PhD degree in 1998 which had been recognized and awarded with the title of the best PhD Thesis in the field of engineering. He has participated in 25 research projects (7 were organized by the Spanish government, 9 by the government of the Canary Islands and 9 by private companies). He was the principal investigator in three of them.

José Luis Calvo Rolle received M.S. and Ph.D. degrees in Industrial Engineering from the University of Leon in 2004 and 2007, respectively. He is an Associate Professor of Automatic Control and the head of the Industrial Engineering Department, Faculty of Engineering, University of A Coruña, Spain. His main research areas are associated with the application of expert system technologies in diagnosis and control systems and in intelligent training systems for control engineering,